Journal of Computational Physics **148,** 527–544 (1999)
Article ID jcph.1998.6128, available online at http://www.idealibrary.com on IDEAL®

A Numerical Solution of the Kinetic Collection Equation Using High Spectral Grid Resolution: A Proposed Reference

Shalva Tzivion, Tamir G. Reisin, and Zev Levin[1]

Department of Geophysics and Planetary Sciences, Raymond and Beverly Sackler Faculty of Exact Sciences, Tel Aviv University, Israel
E-mail: tzivion@snow.tau.ac.il, tamir@storm.tau.ac.il, zev@hail.tau.ac.il

Received February 19, 1998; revised October 19, 1998

The multi-moments method of S. Tzivion, G. Feingold, and Z. Levin was applied to the original kinetic collection equation in order to obtain a set of equations with respect to moments in spectral bins. For solving this set of equations an accurate and efficient method is proposed. The method conserves total mass independently of the number of bins, time step, initial conditions, or kernel of interaction. In the present paper the number of bins was varied from 36, 72, 108, and 144 in order to study the behavior of the solutions. Different kernels and initial conditions were tested. In all cases the results show that when the number of bins increases from 36 to 144 the numerical solution of the KCE gradually converges. Increasing the number of bins from 108 to 144 produces only a small difference in the numerical solution, indicating that the solution obtained for 144 bins approaches the "real" solution of the KCE. The use of this solution for evaluating the accuracy of other numerical methods that solve the KCE is suggested.

Key Words: kinetic collection equation; numerical solutions of integro-differential equations.

1. INTRODUCTION

Growth of particles by the collection of others is of interest in many areas of physics, chemistry, atmospheric, and environmental sciences (e.g., growth of drops in a cloud, capture of aerosols by drops). In spite of its importance, an exact solution to the equation that describes this process using real kernels has not been found. In this paper the growth of particles by collection is addressed and a method is proposed that may be utilized as a reference for evaluating the accuracy of other numerical methods when real kernels are used.

[1] Corresponding author.

0021-9991/99 $30.00

During the last 20 years great efforts were invested in trying to solve the kinetic collection equation (KCE) by developing analytical methods for simplified kernels or by developing numerical methods whenever real kernels were used. Analytical solutions were found for kernels that do not depend on the particles' mass or for those that are proportional to the sum of the masses of the interacting particles (Golovin [11]).

It is normal practice testing the accuracy of a numerical method by comparing its solution to that of an analytical one. Since analytical solutions for the KCE are available only for a few cases, it is customary to assume that agreement between the numerical solution to the analytical one guarantees the correctness of the numerical solution when real kernels are used (e.g., [1, 23]). Unfortunately, this assumption is not always correct since many of the numerical methods agree well with the analytical solutions when special kernels are used, but differ significantly one from the other when a real kernel is used. In fact, there is no method available to reliably verify the numerical results obtained when real kernels are used.

Numerical simulations of the stochastic process of coagulation can be performed using the Monte-Carlo method or by solving the KCE. The justification for using the KCE to describe the stochastic process is out of the scope of the present article and was extensively treated in the literature [8, 9, 20, 21]. In the following paragraphs some previous Monte-Carlo simulations and two numerical methods used for solving the KCE are briefly described.

Monte-Carlo simulations. The stochastic process of coagulation was treated in a number of papers using Monte-Carlo method (e.g., Gillespie [10]). The disadvantage of the method is that for simulating the evolution of the distribution function it is necessary to maintain, during all stages of the simulation, a large number of particles in the volume. This requires extremely large memory and computing time. For this reason this method is not very useful, even for the purpose of evaluating the accuracy of other numerical methods. Seesselberg *et al.* [22] suggested a modified algorithm based on the Monte-Carlo method. Even though this proposed method significantly reduces the amount of computer memory required, it requires large computation time and, therefore, it is not useful even for one-dimensional models. Unfortunately, Seesselberg *et al.* [22] did not provide any indication as to how close their results are to those of Gillespie [10]. In addition, their paper did not present any sensitivity tests with respect to the number of bins, the kernel used, the time step, or the initial conditions. Their only test was a comparison with the analytical solution using Golovin's kernel and, even in this case, only for conditions with relatively low mass content (1 gkg^{-1}). For this reason, although their results are interesting, they could not be considered a benchmark for comparing the accuracy of other methods.

Discrete points methods. In these methods the overall particle spectrum is represented by a number of discrete points, each having an equation which has been transformed from the KCE. In order to calculate the collision integrals it is necessary to prescribe the distribution function itself. Berry and Reinhardt [1] formulated an approximation using a six-point Lagrangian polynomial. This method presents a very good agreement with the analytical solution of Golovin's kernel using small time steps (1–3 s). However, it does not satisfactorily conserve total mass for real kernels, especially for grids where the mass doubles every successive discrete point. In this case, more than 20% of the mass is lost after 7.5 min of simulation [15]. Signeur *et al.* [23] published results from three different numerical methods: (a) discrete spectral points with cubic spline interpolation; (b) discrete spectral bins in which an approximation of the distribution function, using only one moment; (c) a parameterization method. In their simulations a constant, Golovin, or brownian kernel was used and the

size of the particles was varied over a relatively narrow range ($d = 0.01 - 10\ \mu$m). Under these conditions the coagulation process was very slow. Convergence of the first method as a function of the number of spectral bins was used for estimating the accuracy of the parameterization scheme. Any conclusions with respect to the convergence or accuracy of the method, however, cannot be drawn because their tests were limited mostly to cases with slow mass transfer rate. Other works that also used a cubic spline approximation [5, 7], but for a broad spectrum and faster coagulation rate showed a significant lack of total mass conservation, even after short simulation times (≈10–20 min). Unfortunately, results for these last methods were only published for a constant or Golovin's kernels. It is reasonable to conclude that for a real kernel and larger simulation times, the lack of mass conservation would be much greater.

Moment methods. In these methods the overall particle spectrum is divided into discrete bins and the KCE is transformed into a set of equations for moments in each bin. When the approximation uses only one moment, Bleck's method [2] is obtained. By approximating the distribution function with a power polynomial, using more than one moment, the multi-moments method (MMM) is obtained [26]. In contrast to the discrete spectral points methods, the moment methods exactly conserve total mass independently of the number of bins, time step, initial conditions, or kernel of interaction. The limitation of these methods relates to the fact that, by approximating the distribution function by moments, mass is distributed throughout the width of the bins that are otherwise not completely full. Therefore, during the early stages of coagulation, when the size distribution is narrow, moment methods will accelerate the coagulation process. The extent of this acceleration depends on the order of the polynomial used in the approximation in each bin and on the resolution (number of bins).

Although checking the mass conservation of a numerical method is trivial, the evaluation of the relative accuracy of the solution for any initial conditions and kernels is still today a serious difficulty. This is because there is no exact solution that can be used as a "reference" for comparison with various numerical solutions.

The purpose of this work is to develop an accurate numerical solution of the KCE based on the MMM. It will be shown that the numerical solution of the KCE converges to the exact solution when the spectral resolution (number of bins) is gradually increased. It is suggested that this solution may be used as a reference for evaluating the accuracy of various numerical methods. Since calculation time required by the proposed method is acceptable, it can also be implemented into larger models (e.g., multidimensional cloud models).

In Section 2 the set of equations for the moments is obtained and in Section 3 their solution is shown. Results and discussion of the simulations are presented in Section 4 and conclusions in Section 5. Appendix A includes the detail expressions of the moments equations developed in Section 2, and Appendix B discusses the convergence of the numerical solution to the exact solution.

2. EQUATIONS FOR THE MOMENTS

The KCE for a spectrum of particles can be written in the form (also known as Smoluchowski equation):

$$\frac{\partial f(m,t)}{\partial t} = \int_0^{m/2} f(m-x,t)\, f(x,t)\sigma(m-x,x)\, dx - f(m,t) \int_0^{\infty} f(x,t)\sigma(m,x)\, dx, \tag{1}$$

where $f(m,t)\,dm$ is the number of particles with masses between m and $m+dm$ per unit volume at time t. The kernel of interaction $\sigma(m,t)$ represents the probability of collection between particles having mass m and x per unit time, per unit volume of air. The first term on the right-hand side of Eq. (1) represents the gain term for particles with mass m as a result of coagulation of particles with mass $m-x$ and x. The second term is for the loss of particles with mass m due to their growth by collection of other particles. Equation (1) was formulated by Smoluchowski [24] to describe homogeneous coagulation of particles in brownian motion and it implicitily assumes that mass is conserved in the process. A detailed discussion of the solution and properties of this equation can be founded in Voloshtsuk and Sedunov [28] and Melzak [16].

For the numerical solution of this equation, the particle spectrum is divided into discrete bins as

$$m_{k+1} = pm_k, \quad p = \text{const} > 1,$$

where k is the bin number and m_k and m_{k+1} are the lower and upper boundaries of the kth bin, respectively. The width of the bin is represented by the parameter p.

From Eq. (1) a set of equations is obtained for the J moment of the distribution function at bin $k-M_k^J(t)$, defined as

$$M_k^J(t) = \int_{m_k}^{m_{k+1}} m^J f_k(m,t)\,dm. \tag{2}$$

When $J=0$, 1, and 2 one obtains the physical moments of number concentration—$N_k(t)$, mass concentration—$M_k(t)$ and $Z_k(t)$ (radar reflectivity in the case of a cloud), respectively. The set of equations for the particular cases in which $p \geq 2$, $p=2^{1/2}$, $2^{1/3}$, and $2^{1/4}$ are shown in Appendix A (Eqs. (A5), (A6), (A7), and (A8), respectively). These equations are accurate transformations of the initial equation (1) without any mathematical or physical assumptions (following Bleck's method [2] and Tzivion *et al.* [26]). Note that the set of equations was formulated such that each double integral includes interaction between two bins only.

Bleck [2] solved the set of equations derived from (2) for only one moment, assuming a mass-weighted mean value for the drop number density in each category. Since the equations are normalized for the mass density distribution, they conserve the mass content of the spectrum. The main disadvantage of this method is the acceleration of the spectrum development. This acceleration is an artifact of all one-moment approximations since they require the average mass of particles in each bin to be constant and independent of time (usually at the center of the bins). The introduction of weighting functions does not solve the problem since it just moves the position of the average mass but still keeps it constant. It reality, the average mass in a bin can change significantly with time, especially in the bins representing the large particles which tend to be broad because of the logarithmically increasing mass scale.

To overcome these aforementioned problems at least a two-moment approximation method is required. In this case, the average mass in the bin is no longer restricted to be constant. The solution presented by Tzivion *et al.* [26] solves for the first two moments of the mass distribution function for the particular case in which $p=2$. In this article the method is generalized to calculate the coagulation process for any division of the spectrum.

In order to solve this set of equations $f_k(m,t)$ is approximated by its moments. Usually, this approximation is implemented using Legendre orthogonal polynoms [4]. The main deficiency of such an approach is that this approximation cannot assure the positiveness of the distribution function within the interval of approximation. In this work $f_k(m,t)$ is approximated by two consecutive moments as in Tzivion *et al.* [26]. In this case the approximation is given by

$$m^J f_k(m,t) = \frac{m_k^J}{(p-1)} f_k(m_k,t)\left(p - \frac{m}{m_k}\right) + \frac{m_{k+1}^J}{(p-1)} f_k(m_{k+1},t)\left(\frac{m}{m_k} - 1\right). \quad (3)$$

With this approximation, the positiveness of $m^J f_k(m,t)$ is guaranteed if $f_k(m_k,t)$ and $f_k(m_{k+1},t)$ are positive.

Using (2) and (3) one can solve for $f_k(m_k,t)$ and $f_k(m_{k+1},t)$ as a function of two moments $N_k(t)$ and $M_k(t)$,

$$\begin{aligned} f_k(m_k,t) &= \frac{2N_k(t)}{(p-1)^2 m_k}\left[p - \frac{\bar{m}_k(t)}{m_k}\right] \\ f_k(m_{k+1},t) &= \frac{2N_k(t)}{(p-1)^2 m_k}\left[\frac{\bar{m}_k(t)}{m_k} - 1\right], \end{aligned} \quad (4)$$

where

$$\bar{m}_k(t) = \frac{M_k(t)}{N_k(t)}$$

is the average mass in bin k.

Alternatively, higher order moments can be used to express $f_k(m_k,t)$ and $f_k(m_{k+1},t)$. Similarly to Eq. (4), when using $M_k(t)$ and $Z_k(t)$ one obtains

$$\begin{aligned} f_k(m_k,t) &= \frac{2[pm_k M_k(t) - Z_k(t)]}{(p-1)^2 m_k^3} \\ f_k(m_{k+1},t) &= \frac{2[Z_k(t) - m_k M_k(t)]}{p(p-1)^2 m_k^3}. \end{aligned} \quad (5)$$

In order to solve (A5)–(A8) for moments $N_k(t)$ and $M_k(t)$, one needs to close the set of equations by setting $Z_k(t)$ in (5) as a function of the first two moments. For that purpose a nondimensional parameter ξ that relates three neighboring moments of the distribution in the kth bin is introduced (for details see [26]):

$$\xi = \frac{\int_{m_k}^{m_{k+1}} m^{J+1} f(m,t)\,dx \int_{m_k}^{m_{k+1}} m^{J-1} f(m,t)\,dx}{\left[\int_{m_k}^{m_{k+1}} m^J f(m,t)\,dx\right]^2}. \quad (6)$$

As shown in [26] the value of this parameter is bounded by

$$1 \le \xi \le \frac{(p+1)^2}{4p}; \quad (7)$$

by decreasing the parameter p (i.e., increasing the number of bins) it is possible, in principle, to approximate moments in a bin of order greater than J by moments in the same bin, of order not exceeding J, to any required degree of accuracy.

For $1 \le p \le 2$, ξ varies very little (e.g., for $p = 2$, ξ varies between 1 and 1.125 and for $p = 2^{1/3}$ it varies between 1 and 1.013); therefore it can be averaged with sufficient accuracy as

$$\bar{\xi} = 0.5\left[1 + (p+1)\frac{m_k}{\bar{m}_k(t)} - p\left(\frac{m_k}{\bar{m}_k(t)}\right)^2\right]. \tag{8}$$

Recursively using the $\bar{\xi}$ parameter $M_k^J(t)$ can be expressed as a function of the two first moments in the kth bin as

$$M_k^J(t) = \bar{\xi}^{J(J-1)/2}\bar{m}_k^{J-1}(t)M_k(t). \tag{9}$$

Note that in order to use (8) it is necessary that $m_k \le \bar{m}_k(t) \le m_{k+1}$. In case these conditions are not fulfilled (because of inaccuracies associated with the numerical scheme), one requires $\bar{\xi}$ to equal 1. Using (8) and (9), Eq. (5) can be rewritten as

$$\begin{aligned} f_k(m_k, t) &= \frac{2N_k(t)}{(p-1)^2 m_k}\left[(p-1)\left(\frac{\bar{m}_k(t)}{m_k}\right) - \left(\frac{\bar{m}_k(t)}{m_k}\right)^2 + p\right] \\ f_k(m_{k+1}, t) &= \frac{2N_k(t)}{(p-1)^2 m_k}\left[(p-1)\left(\frac{\bar{m}_k(t)}{m_k}\right) + \left(\frac{\bar{m}_k(t)}{m_k}\right)^2 - p\right] \end{aligned} \tag{10}$$

In the integrals in which $f_k(m, t)$ appears the approximation is done using (4) while if $m f_k(m, t)$ appears (10) is used. In (4) and (10), $f_k(m_k, t)$ and $f_k(m_{k+1}, t)$ will be positive within bin k if the trivial condition $m_k \le \bar{m}_k(t) \le m_{k+1}$ is fullfiled. If because of numerical truncation errors this is not the case, one requires that

$$\begin{aligned} &f_k(m_k, t) = 2\frac{N_k(t)}{(p-1)m_k}, \quad f_k(m_{k+1}, t) = 0, \quad \text{if } \bar{m}_k(t) < m_k, \\ &f_k(m_k, t) = 0, \quad f_k(m_{k+1}, t) = 2\frac{N_k(t)}{(p-1)m_k}, \quad \text{if } \bar{m}_k(t) > m_{k+1}. \end{aligned} \tag{11}$$

3. THE SOLUTION OF THE EQUATIONS

Equations (A5)–(A8) are written for two physical moments in *each bin*. By introducing the approximation for the distribution function (Eq. (3)) in the inner and outer integrals, a set of equations is obtained in which the time-dependent functions are out of the integrals. The expressions under the integrals are of the type $m^n x^l \sigma(m, x)$ $(n, l = 0, 1, 2, 3)$ in which all the functions are known. These double integrals can be calculated a priori only once and then tabulated for use during the running of the model. This procedure is also applicable to cases when the kernel depends on time, as long as it can be approximated as a function of mass multiplied by a function of time. Finally, a set of differential equations is obtained with the general form

$$\frac{dM_k^J(t)}{dt} = F_k^J(t) \tag{12}$$

with a solution:

$$M_k^J(t + \Delta t) = M_k^J(t) + \Delta t F_k^J(t). \tag{13}$$

The accuracy of the numerical solution of these ordinary differential equations depends only on the spectral resolution and time step. For a small time step and high resolution the numerical solution aspires to the exact solution [12, 14, 19].

For the case in which $p \geq 2$ a more accurate solution can be obtained. In this case, all the outer integrals are over full bins and only some of the inner integrals are over incomplete bins. The approximation of the distribution function is, therefore, carried out only when the inner integral is over an incomplete bin. As the coagulation proceeds the distribution function changes significantly. One can, therefore, expect that by avoiding the approximation of the distribution function, the accuracy of the solution will increase. In these cases, in order to close the set of equations with respect to the moments, the kernel $\sigma(m, x)$ is approximated. Since this is a known function, it can be approximated to any desired accuracy. This approach is *recommended* for $p \geq 2$ if a slightly better accuracy is required. Similar satisfactory results can be obtained by introducing the approximation of the distribution function in both the inner and outer integrals.

For the special case of $p = 2$, (A5) is identical to (5) in Tzivion *et al.* [26]. In this case the approximation of the distribution function is only required in the inner integral of the first and third terms on the right-hand side (RHS). The kernel is approximated according to

$$\sigma_{k,i}(m, x) = \tilde{\sigma}_{k,i}(m + x), \tag{14}$$

where

$$\tilde{\sigma}_{k,i} = \frac{1}{(x_{i+1} - x_i)(m_{k+1} - m_k)} \int_{x_i}^{x_{i+1}} dx \int_{m_k}^{m_{k+1}} \frac{\sigma_{k,i}(m, x)}{(m + x)}\, dm. \tag{15}$$

After introducing (14) into (A5) a set of equations is obtained for $M_k^J(t)$ which is not closed because higher moments appear on the RHS of the equations. By using the expressions given in (8) and (9) the set of equations can be closed.

The question still remains: how can one be sure that the solution obtained using a real kernel *is indeed* the real one? In Appendix B this point is discussed and it is shown that when the resolution increases and the solution converges, it converges to the real solution.

Numerical simulations were conducted for three different kernels: Golovin's [11] $\sigma(m, x) = 1500(m + x)$, which has an analytical solution; and Long's [15] and Hall's [13] coalescence efficiencies for the hydrodynamical kernel (hereafter Long and Hall kernels, respectively). For Golovin's kernel the convergence of the numerical solutions to the analytical one was checked using different width parameters, p, and different time steps, Δt. In all the simulations, an exponential initial distribution was used, with a mass concentration of 1–3 gkg^{-1} and number concentration of 300 cm^{-3}. Note that in this paper mass refers to that of water drops, namely density of 1 gcm^{-3}. Simulations were carried out for $p = 2$ (36 bins), $p = 2^{1/2}$ (72 bins), $p = 2^{1/3}$ (108 bins), and $p = 2^{1/4}$ (144 bins). In all the cases the minimum radius was 1.5625 μm. The time step in the simulations varied between 1, 2, 5, and 10 s. The results presented in the plots (except Fig. 7) are for time step of 1 s.

Figure 1 shows the evolution of the spectrum by collection after 20 and 40 min, respectively; as given by the analytical solution and by the MMM for 36, 72, 108, and 144 bins, in the case of Golovin kernel. In these cases the average radius of the initial distribution was $\bar{r}_0 = 9.3$ μm which corresponds to mass concentration of 1 gkg^{-1} for water drops. Figure 2 is similar to Fig. 1 but for an initial average radius of $\bar{r}_0 = 13.4$ μm (3 gkg^{-1}), after 10 and 15 min, respectively. From these figures one sees a small acceleration for 36 and 72 bins

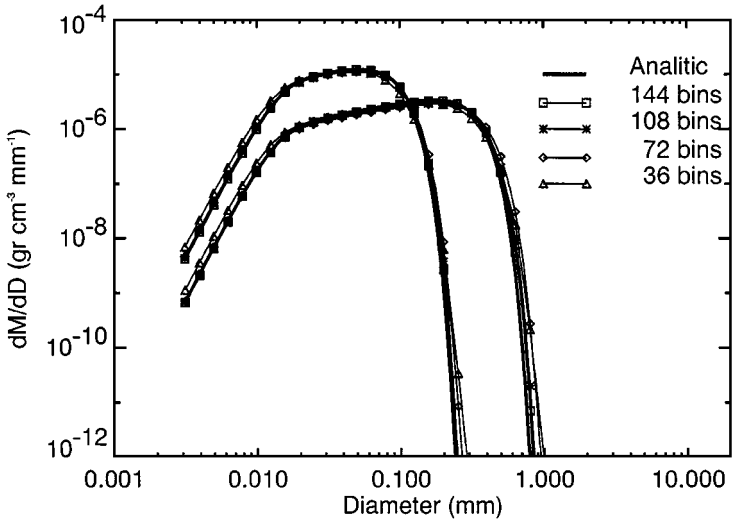

FIG. 1. Mass distribution as a function of diameter for different spectral resolutions using Golovin's kernel, after 20 and 40 min of simulation. The average radius of the initial distribution was 9.3 μm (1 gkg^{-1}). The time step was 1 s.

and very good agreement for 108 and 144 bins, as compared to the analytical solution. In all cases the total mass was fully conserved regardless the number of bins or the time step.

Figures 3 and 4 present the evolution of the number and mass concentration after 20 and 40 min, respectively; in case of Long's kernel. In these cases the initial average radius was $\bar{r}_0 = 9.3$ μm. Figures 5 and 6 are similar to Figs. 3 and 4 but for an initial average radius of $\bar{r}_0 = 13.4$ μm (3 gkg^{-1}). From Figs. 3–6 it can be seen that a moderate acceleration appeared for 36 and 72 bins, as compared to the 144 bins case, while the 108 bins converged to the 144. This acceleration phenomena is very small when one looks at the graph representing

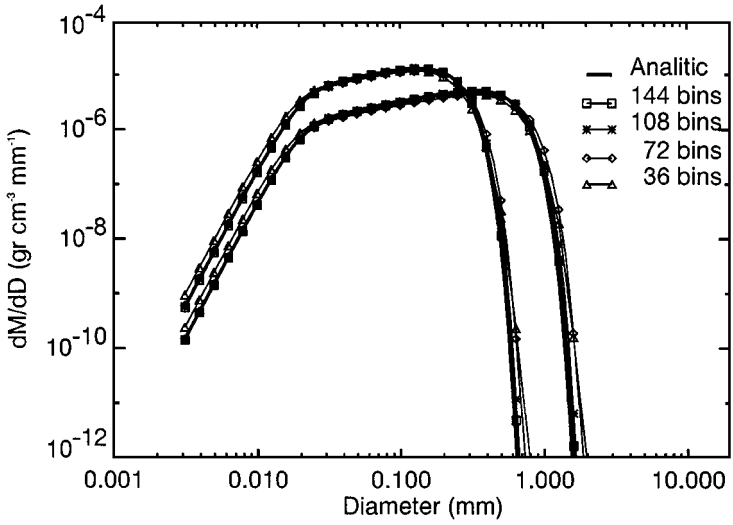

FIG. 2. Mass distribution as a function of diameter for different spectral resolutions using Golovins's kernel, after 10 and 15 min of simulation. The average radius of the initial distribution was 13.4 μm (3 gkg^{-1}). The time step was 1 s.

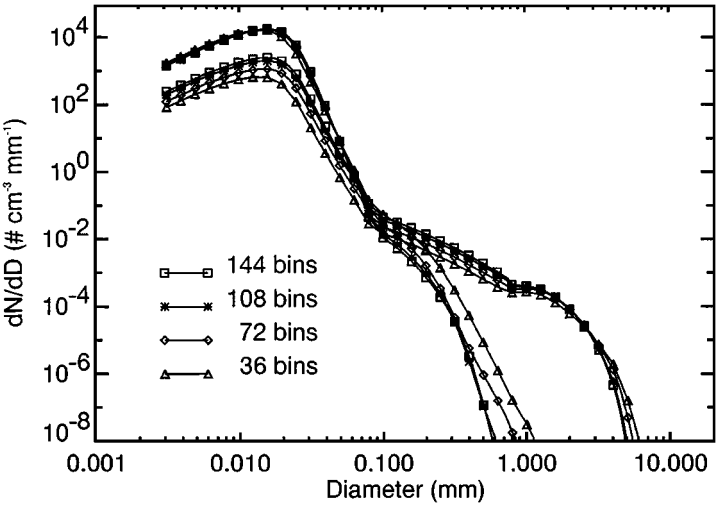

FIG. 3. Number concentration distribution as a function of diameter for different spectral resolutions using Long's kernel after 20 and 40 min of simulation. The average radius of the initial distribution was 9.3 μm (1 gkg^{-1}). The time step was 1 s.

number (or concentration) distribution, but it increases when the higher moments, such as the mass distribution, are viewed. Also, for Long's kernel total mass conservation was independent of the time step (1–10 s) and number of bins. Note that the convergence of the case with 108 bins to that of the 144 bins did not depend on the initial distribution.

From Figs. 3–6 it can be seen that at later times the convergence to the 144 bins solution is better than at the earlier stages of spectra evolution. The reason is that at the early stages the growth by collection puts particles into empty bins, usually at the lower end of each bin. The approximation of the distribution function by moments spreads the mass over the whole bin and thus artificially accelerates the growth. At a later stage (the mature stage of

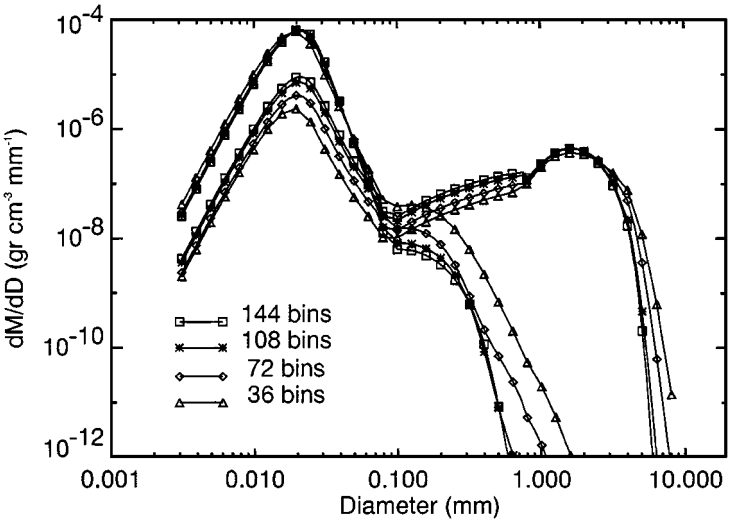

FIG. 4. Like Fig. 3, for mass distribution.

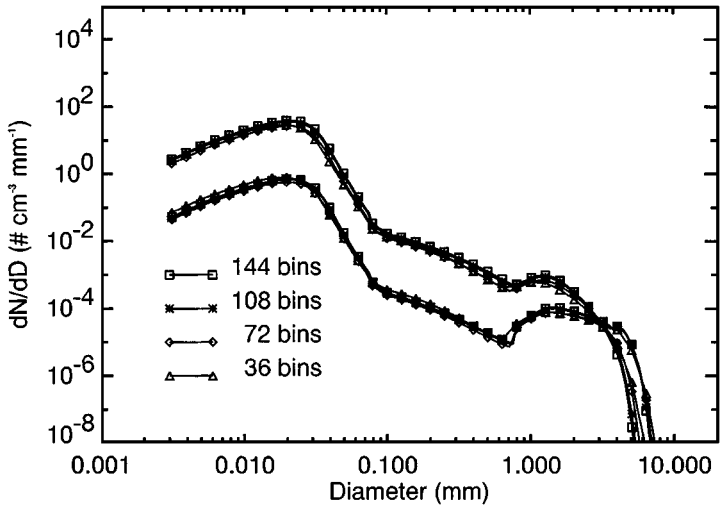

FIG. 5. Number concentration distribution as a function of diameter for different spectral resolutions using Long's kernel, after 10 and 15 min of simulation. The average radius of the initial distribution was 13.4 μm (3 gkg^{-1}). The time step was 1 s.

the spectrum), the growth by collection often places the particles at the upper end of the bins and the approximation tends to decelerate the growth. At the same time one sees that the rate of convergence also depends on the initial distribution. It increases when the initial average radius increases.

The convergence of higher moments (e.g., $Z_k(t)$) was also tested and found to be similar to those obtained for the mass concentration.

In Fig. 7 the results obtained for different time steps are shown, in the case of Long's kernel for 144 bins, with 1 gkg^{-1} at two times: 20 min and 40 min. For time steps as 1 and 2 s, the results are almost identical while for 5 s and 10 s the accuracy is somewhat lower.

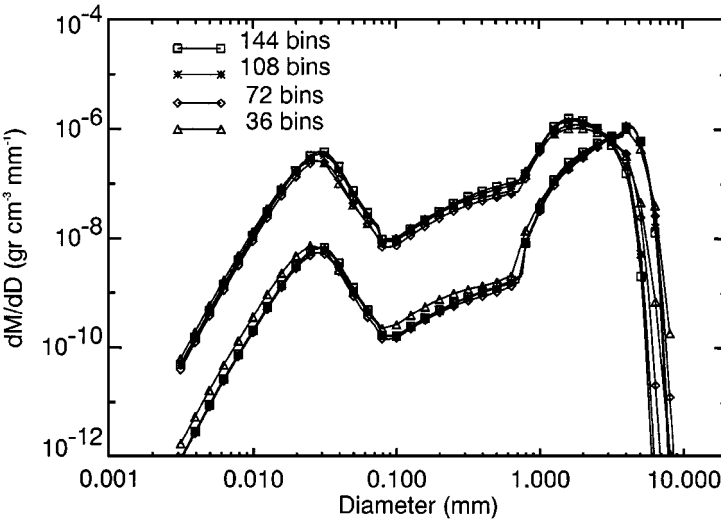

FIG. 6. Like Fig. 5, for mass distribution.

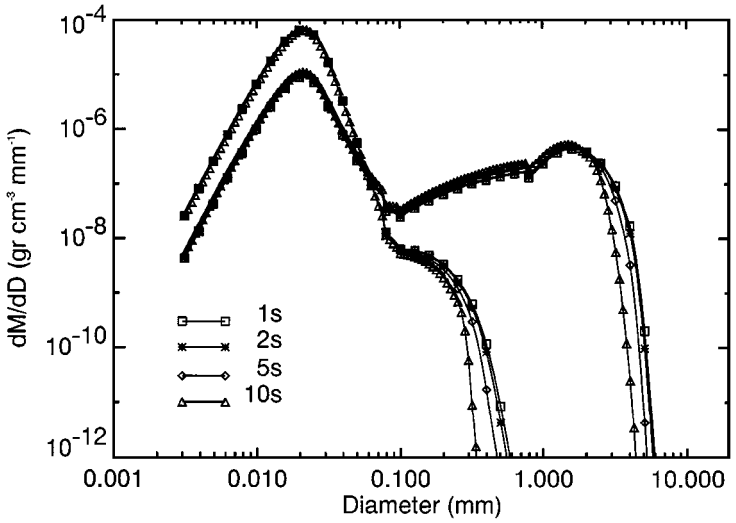

FIG. 7. Mass distribution as a function of diameter for Long's kernel using different time steps. The number of bins was 144 and the average radius of the initial distribution was 9.3 μm (1 gkg^{-1}).

One can, therefore, conclude that a time step of 1 s be utilized when using the 144-bin algorithm as a reference for comparison with other numerical methods. As already pointed out, total mass is accurately conserved for all time steps.

Figure 8 is similar to Fig. 6, except that here Hall's kernel was used. From this figure it can be seen that the results are very similar to those obtained using Long's kernel. Only small differences appear in the coagulation and convergence rates. In this case the coagulation rate is very slightly smaller than when Long's kernel is used. Using Hall's kernel rather than Long's kernel a little better convergence of the 108 bins to 144 bins is obtained.

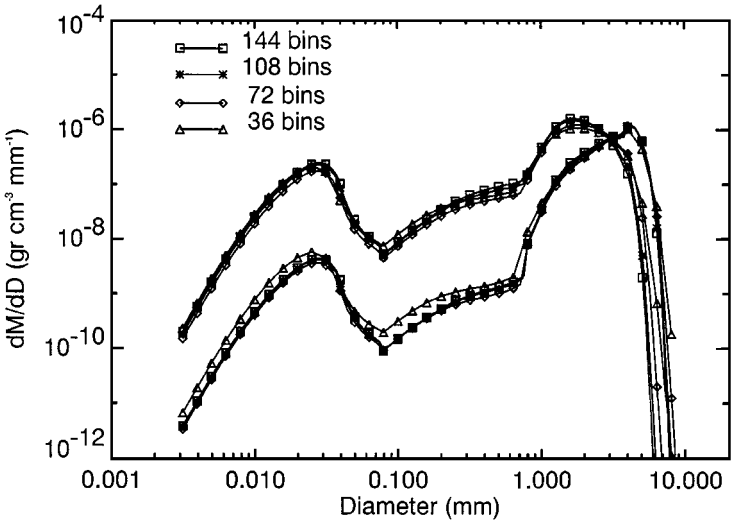

FIG. 8. Mass concentration distribution as a function of diameter for Hall's kernel using different spectral resolutions, after 10 and 15 min of simulation. The average radius of the initial distribution was 13.4 μm (1 gkg^{-1}). The time step was 1 s.

5. CONCLUSIONS

In this paper the solution of the kinetic collection equation was investigated using the multi-moments method with 36, 72, 108, and 144 bins. The total mass was exactly conserved without dependence on the initial conditions, resolution, time step, or kernel. Three different kernels were used: Golovin's kernel, to which an analytical solution is available, and the real kernels of Long and Hall. It was shown that, as the number of bins increased, better convergence to that of the 144 bins was obtained. The results from 108 bins were almost identical to those obtained with 144 bins.

Based on these results it is inferred that the solution obtained for 144 bins approaches the exact solution of the KCE for any kernel of interaction and it could be utilized as a reference for evaluating the accuracy of other numerical methods used for computing the kinetic collection equation.

It is important to note that the same method of moments has been used to develop numerical solutions for different kinetic transfer equations such as for the growth of cloud drops by vapor diffusion [27] for describing the changes in the raindrop size spectra due to collisional breakup [6] and for treating the interactions between drops and ice particles [18]. Furthermore, the method of moments can be used to solve a variety of physical processes described by integro–differential equations.

The numerical calculations of the coagulation process using 144 bins and 1 s time step, required about 300 s of CPU time on a SGI Challenge R10000 for simulating 1 h. Therefore, in simulations in which a detailed description of the coagulation process is required, the very high resolution grid can be implemented.

The computer codes that implement the algorithms presented in this article can be freely obtained on the internet at http://www.tau.ac.il/geophysics/staff/tamir1/mom.html.

APPENDIX A

Using the KCE (1) and Eq. (2), one can obtain a system of equations with respect to the moments in each bin k of the size distribution as

$$\frac{dM_k^J(t)}{dt} = \int_{m_k}^{m_{k+1}} m^J\,dm \int_{m_1}^{m/2} f(m-x,t)\,f(m,x)\sigma(m-x,x)\,dx - \sum_{i=1}^{I}\int_{x_i}^{x_{i+1}} f_i(x,t)\,dx \int_{m_k}^{m_{k+1}} m^J\,f_k(m,t)\,dm, \tag{A1}$$

where I is the total number of bins and m_1, the smallest mass considered. The first double integral (gain integral) in Eq. (A1) is transformed by dividing the area of integration into separate subareas in which f_k and f_i represent the size distributions in bins k and i, respectively (for details see [2, 26]).

Using this approach a set of equations is obtained for the particular cases used in this paper. Equation (A5) is derived for $p \geq 2$, Eq. (A6) is derived for $p = 2^{1/2}$, Eq. (A7) is derived for $p = 2^{1/3}$, and Eq. (A8) is derived for $p = 2^{1/4}$.

For the minimum and maximum values of the drop radii we chose $r_1 = 1.5625\ \mu$m and $r_{\max} = 6.4$ mm. Using different values of p, as above, within this size range the number of bins, I, varies from $I \leq 36$, $I = 72$, $I = 108$, and $I = 144$, as represented by Eqs. (A5),

(A6), (A7), and (A8), respectively. The notation used is:

$$\mathcal{F}^J_{k,i}(m,x,t) = (m+x)^J f_k(m,t) f_i(x,t)\sigma_{k,i}(m,x) \tag{A2}$$

$$\mathcal{G}^J_{k,i}(m,x,t) = [(m+x)^J - m^J] f_k(m,t) f_i(x,t)\sigma_{k,i}(m,x) \tag{A3}$$

$$\mathcal{H}^J_{k,i}(m,x,t) = m^J f_k(m,t) f_i(x,t)\sigma_{i,k}(x,m); \tag{A4}$$

$p \geq 2$,

$$\begin{aligned}
\frac{dM^J_k(t)}{dt} &= \left[\sum_{i=1}^{k-2}\int_{x_i}^{x_{i+1}}\int_{m_k-x}^{m_k}\mathcal{F}^J_{k-1,i}(m,x,t)\,dx\,dm + 0.5\int_{x_k/2}^{x_k}\int_{m_k/2}^{m_k}\mathcal{F}^J_{k-1,k-1}(m,x,t)\,dx\,dm\right] \\
&\quad - \left[\sum_{i=1}^{k-1}\int_{x_i}^{x_{i+1}}\int_{m_{k+1}-x}^{m_{k+1}}\mathcal{F}^J_{k,i}(m,x,t)\,dx\,dm + 0.5\int_{x_{k+1}/2}^{x_{k+1}}\int_{m_{k+1}/2}^{m_{k+1}}\mathcal{F}^J_{k,k}(m,x,t)\,dx\,dm\right] \\
&\quad + \left[\sum_{i=1}^{k-1}\int_{x_i}^{x_{i+1}}\int_{m_k}^{m_{k+1}}\mathcal{G}^J_{k,i}(m,x,t)\,dx\,dm - \sum_{i=k}^{I}\int_{x_i}^{x_{i+1}}\int_{m_k}^{m_{k+1}}\mathcal{H}^J_{k,i}(m,x,t)\,dx\,dm\right] \\
&\quad + \left[\int_{x_{k-1}}^{x_k/2}\int_{m_k-x}^{m_k}\mathcal{F}^J_{k-1,k-1}(m,x,t)\,dx\,dm - \int_{x_k}^{x_{k+1}/2}\int_{m_{k+1}-x}^{m_{k+1}}\mathcal{F}^J_{k,k}(m,x,t)\,dx\,dm\right] \\
&\quad + 0.5\int_{x_k}^{x_{k+1}}\int_{m_k}^{m_{k+1}}\mathcal{F}^J_{k,k}(m,x,t)\,dx\,dm;
\end{aligned} \tag{A5}$$

$p = 2^{1/2}$,

$$\begin{aligned}
\frac{dM^J_k(t)}{dt} &= \left[\sum_{i=1}^{k-5}\int_{x_i}^{x_{i+1}}\int_{m_k-x}^{m_k}\mathcal{F}^J_{k-1,i}(m,x,t)\,dx\,dm + \int_{x_{k-4}}^{x_k-x_{k-1}}\int_{m_k-x}^{m_k}\mathcal{F}^J_{k-1,k-4}(m,x,t)\,dx\,dm\right] \\
&\quad - \left[\sum_{i=1}^{k-4}\int_{x_i}^{x_{i+1}}\int_{m_{k+1}-x}^{m_{k+1}}\mathcal{F}^J_{k,i}(m,x,t)\,dx\,dm + \int_{x_k-3}^{x_{k+1}-x_k}\int_{m_{k+1}-x}^{m_{k+1}}\mathcal{F}^J_{k,k-3}(m,x,t)\,dx\,dm\right] \\
&\quad + \left[\sum_{i=1}^{k-4}\int_{x_i}^{x_{i+1}}\int_{m_k}^{m_{k+1}}\mathcal{G}^J_{k,i}(m,x,t)\,dx\,dm - \sum_{i=\max(1,k-3)}^{I}\int_{x_i}^{x_{i+1}}\int_{m_k}^{m_{k+1}}\mathcal{H}^J_{k,i}(m,x,t)\,dx\,dm\right] \\
&\quad + \int_{x_{k-3}}^{x_{k+1}-x_k}\int_{m_k}^{m_{k+1}-x}\mathcal{F}^J_{k,k-3}(m,x,t)\,dx\,dm + \left[\int_{x_k-x_{k-1}}^{x_{k-3}}\int_{m_{k-1}}^{m_k}\mathcal{F}^J_{k-1,k-4}(m,x,t)\,dx\,dm\right. \\
&\quad + \int_{x_{k-3}}^{x_{k+1}-x_k}\int_{m_{k-1}}^{m_k}\mathcal{F}^J_{k-1,k-3}(m,x,t)\,dx\,dm + \int_{x_{k+1}-x_k}^{x_{k-2}}\int_{m_{k-1}}^{m_{k+1}-x}\mathcal{F}^J_{k-1,k-3}(m,x,t)\,dx\,dm \\
&\quad \left.+ \int_{x_{k-2}}^{x_{k-1}}\int_{m_{k-1}}^{m_{k+1}-x}\mathcal{F}^J_{k-1,k-2}(m,x,t)\,dx\,dm\right] + \left[\int_{x_k-x_{k-1}}^{x_{k-3}}\int_{m_k-x}^{m_{k-1}}\mathcal{F}^J_{k-2,k-4}(m,x,t)\,dx\,dm\right. \\
&\quad \left.+ \int_{x_{k-3}}^{x_{k-2}}\int_{m_k-x}^{m_{k-1}}\mathcal{F}^J_{k-2,k-3}(m,x,t)\,dx\,dm + 0.5\int_{x_{k-2}}^{x_{k-1}}\int_{m_{k-2}}^{m_{k-1}}\mathcal{F}^J_{k-2,k-2}(m,x,t)\,dx\,dm\right];
\end{aligned} \tag{A6}$$

$$p = 2^{1/3},$$

$$\frac{dM_k^J(t)}{dt} =$$

$$\left[\sum_{i=1}^{k-8}\int_{x_i}^{x_{i+1}}\int_{m_k-x}^{m_k}\mathcal{F}_{k-1,i}^J(m,x,t)\,dx\,dm+\int_{x_{k-7}}^{x_k-x_{k-1}}\int_{m_k-x}^{m_k}\mathcal{F}_{k-1,k-7}^J(m,x,t)\,dx\,dm\right]$$
$$-\left[\sum_{i=1}^{k-7}\int_{x_i}^{x_{i+1}}\int_{m_{k+1}-x}^{m_{k+1}}\mathcal{F}_{k,i}^J(m,x,t)\,dx\,dm+\int_{x_{k-6}}^{x_{k+1}-x_k}\int_{m_{k+1}-x}^{m_{k+1}}\mathcal{F}_{k,k-6}^J(m,x,t)\,dx\,dm\right]$$
$$+\left[\sum_{i=1}^{k-7}\int_{x_i}^{x_{i+1}}\int_{m_k}^{m_{k+1}}\mathcal{G}_{k,i}^J(m,x,t)\,dx\,dm-\sum_{i=\max(1,k-8)}^{I}\int_{x_i}^{x_{i+1}}\int_{m_k}^{m_{k+1}}\mathcal{H}_{k,i}^J(m,x,t)\,dx\,dm\right]$$
$$+\int_{x_{k-6}}^{x_{k+1}-x_k}\int_{m_k}^{m_{k+1}}\mathcal{F}_{k,k-6}^J(m,x,t)\,dx\,dm+\left[\int_{x_k-x_{k-1}}^{x_{k-6}}\int_{m_{k-1}}^{m_k}\mathcal{F}_{k-1,k-7}^J(m,x,t)\,dx\,dm\right.$$
$$+\int_{x_{k-6}}^{x_{k+1}-x_k}\int_{m_{k-1}}^{m_k}\mathcal{F}_{k-1,k-6}^J(m,x,t)\,dx\,dm+\int_{x_{k+1}-x_k}^{x_{k-5}}\int_{m_{k-1}}^{m_{k+1}-x}\mathcal{F}_{k-1,k-6}^J(m,x,t)\,dx\,dm$$
$$\left.+\int_{x_{k-5}}^{x_{k-4}}\int_{m_{k-1}}^{m_{k+1}-x}\mathcal{F}_{k-1,k-5}^J(m,x,t)\,dx\,dm+\int_{x_{k+1}-x_{k-1}}^{x_{k-4}}\int_{m_{k-1}}^{m_{k+1}-x}\mathcal{F}_{k-1,k-4}^J(m,x,t)\,dx\,dm\right]$$
$$+\left[\int_{x_k-x_{k-1}}^{x_{k-6}}\int_{m_k-x}^{m_{k-1}}\mathcal{F}_{k-2,k-7}^J(m,x,t)\,dx\,dm+\int_{x_{k-6}}^{x_{k-5}}\int_{m_k-x}^{m_{k-1}}\mathcal{F}_{k-2,k-6}^J(m,x,t)\,dx\,dm\right.$$
$$+\int_{x_{k-5}}^{x_k-x_{k-2}}\int_{m_k-x}^{m_{k-1}}\mathcal{F}_{k-2,k-5}^J(m,x,t)\,dx\,dm+\int_{x_k-x_{k-2}}^{x_{k-4}}\int_{m_{k-2}}^{m_{k-1}}\mathcal{F}_{k-2,k-5}^J(m,x,t)\,dx\,dm$$
$$+\int_{x_{k-4}}^{x_{k+1}-x_{k-1}}\int_{m_{k-2}}^{m_{k-1}}\mathcal{F}_{k-2,k-4}^J(m,x,t)\,dx\,dm+\int_{x_{k+1}-x_{k-1}}^{x_{k-3}}\int_{m_{k-2}}^{m_{k+1}-x}\mathcal{F}_{k-2,k-4}^J(m,x,t)\,dx\,dm$$
$$\left.+\int_{x_{k-3}}^{x_{k-2}}\int_{m_{k-2}}^{m_{k+1}-x}\mathcal{F}_{k-2,k-3}^J(m,x,t)\,dx\,dm\right]+\left[\int_{x_k-x_{k-2}}^{x_{k-4}}\int_{m_k-x}^{m_{k-2}}\mathcal{F}_{k-3,k-5}^J(m,x,t)\,dx\,dm\right.$$
$$\left.+\int_{x_{k-4}}^{x_{k-3}}\int_{m_k-x}^{m_{k-2}}\mathcal{F}_{k-3,k-4}^J(m,x,t)\,dx\,dm+0.5\int_{x_{k-3}}^{x_{k-2}}\int_{m_{k-3}}^{m_{k-2}}\mathcal{F}_{k-3,k-3}^J(m,x,t)\,dx\,dm\right];\tag{A7}$$

$$p = 2^{1/4},$$

$$\frac{dM_k^J(t)}{dt} =$$

$$\left[\sum_{i=1}^{k-12}\int_{x_i}^{x_{i+1}}\int_{m_k-x}^{m_k}\mathcal{F}_{k-1,i}^J(m,x,t)\,dx\,dm+\int_{x_{k-11}}^{x_k-x_{k-1}}\int_{m_k-x}^{m_k}\mathcal{F}_{k-1,k-11}^J(m,x,t)\,dx\,dm\right]$$
$$-\left[\sum_{i=1}^{k-11}\int_{x_i}^{x_{i+1}}\int_{m_{k+1}-x}^{m_{k+1}}\mathcal{F}_{k,i}^J(m,x,t)\,dx\,dm+\int_{x_{k-10}}^{x_{k+1}-x_k}\int_{m_{k+1}-x}^{m_{k+1}}\mathcal{F}_{k,k-10}^J(m,x,t)\,dx\,dm\right]$$
$$+\left[\sum_{i=1}^{k-11}\int_{x_i}^{x_{i+1}}\int_{m_k}^{m_{k+1}}\mathcal{G}_{k,i}^J(m,x,t)\,dx\,dm-\sum_{i=\max(1,k-10)}^{I}\int_{x_i}^{x_{i+1}}\int_{m_k}^{m_{k+1}}\mathcal{H}_{k,i}^J(m,x,t)\,dx\,dm\right]$$

$$+\int_{x_{k-10}}^{x_{k+1}-x_k}\int_{m_k}^{m_{k+1}}\mathcal{F}^J_{k,k-10}(m,x,t)\,dx\,dm+\Bigg[\int_{x_k-x_{k-1}}^{x_{k-10}}\int_{m_{k-1}}^{m_k}\mathcal{F}^J_{k-1,k-11}(m,x,t)\,dx\,dm$$
$$+\int_{x_{k-10}}^{x_{k+1}-x_k}\int_{m_{k-1}}^{m_k}\mathcal{F}^J_{k-1,k-10}(m,x,t)\,dx\,dm+\int_{x_{k+1}-x_k}^{x_{k-9}}\int_{m_{k-1}}^{m_{k+1}-x}\mathcal{F}^J_{k-1,k-10}(m,x,t)\,dx\,dm$$
$$+\int_{x_{k-9}}^{x_{k-8}}\int_{m_{k-1}}^{m_{k+1}-x}\mathcal{F}^J_{k-1,k-9}(m,x,t)\,dx\,dm+\int_{x_{k-8}}^{x_{k-7}}\int_{m_{k-1}}^{m_{k+1}-x}\mathcal{F}^J_{k-1,k-8}(m,x,t)\,dx\,dm$$
$$+\int_{x_{k-7}}^{x_{k+1}-x_{k-1}}\int_{m_{k-1}}^{m_{k+1}-x}\mathcal{F}^J_{k-1,k-7}(m,x,t)\,dx\,dm\Bigg]$$
$$+\Bigg[\int_{x_k-x_{k-1}}^{x_{k-10}}\int_{m_k-x}^{m_{k-1}}\mathcal{F}^J_{k-2,k-11}(m,x,t)\,dx\,dm+\int_{x_{k-10}}^{x_{k-9}}\int_{m_k-x}^{m_{k-1}}\mathcal{F}^J_{k-2,k-10}(m,x,t)\,dx\,dm$$
$$+\int_{x_{k-9}}^{x_{k-8}}\int_{m_k-x}^{m_{k-1}}\mathcal{F}^J_{k-2,k-9}(m,x,t)\,dx\,dm+\int_{x_{k-8}}^{x_k-x_{k-2}}\int_{m_k-x}^{m_{k-1}}\mathcal{F}^J_{k-2,k-8}(m,x,t)\,dx\,dm$$
$$+\int_{x_k-x_{k-2}}^{x_{k-7}}\int_{m_{k-2}}^{m_{k-1}}\mathcal{F}^J_{k-2,k-8}(m,x,t)\,dx\,dm+\int_{x_{k-7}}^{x_{k+1}-x_{k-1}}\int_{m_{k-2}}^{m_{k-1}}\mathcal{F}^J_{k-2,k-7}(m,x,t)\,dx\,dm$$
$$+\int_{x_{k+1}-x_{k-1}}^{x_{k-6}}\int_{m_{k-2}}^{m_{k+1}-x}\mathcal{F}^J_{k-2,k-7}(m,x,t)\,dx\,dm+\int_{x_{k-6}}^{x_{k-5}}\int_{m_{k-2}}^{m_{k+1}-x}\mathcal{F}^J_{k-2,k-6}(m,x,t)\,dx\,dm$$
$$+\int_{x_{k-5}}^{x_{k+1}-x_{k-2}}\int_{m_{k-2}}^{m_{k+1}-x}\mathcal{F}^J_{k-2,k-5}(m,x,t)\,dx\,dm\Bigg]$$
$$+\Bigg[\int_{x_k-x_{k-2}}^{x_{k-7}}\int_{m_k-x}^{m_{k-2}}\mathcal{F}^J_{k-3,k-8}(m,x,t)\,dx\,dm+\int_{x_{k-7}}^{x_{k-6}}\int_{m_k-x}^{m_{k-2}}\mathcal{F}^J_{k-3,k-7}(m,x,t)\,dx\,dm$$
$$+\int_{x_{k-6}}^{x_k-x_{k-3}}\int_{m_k-x}^{m_{k-2}}\mathcal{F}^J_{k-3,k-6}(m,x,t)\,dx\,dm+\int_{x_k-x_{k-3}}^{x_{k-5}}\int_{m_{k-3}}^{m_{k-2}}\mathcal{F}^J_{k-3,k-6}(m,x,t)\,dx\,dm$$
$$+\int_{x_{k-5}}^{x_{k+1}-x_{k-2}}\int_{m_{k-3}}^{m_{k-2}}\mathcal{F}^J_{k-3,k-5}(m,x,t)\,dx\,dm+\int_{x_{k+1}-x_{k-2}}^{x_{k-4}}\int_{m_{k-3}}^{m_{k+1}-x}\mathcal{F}^J_{k-3,k-5}(m,x,t)\,dx\,dm$$
$$+\int_{x_{k-4}}^{x_{k-3}}\int_{m_{k-3}}^{m_{k+1}-x}\mathcal{F}^J_{k-3,k-4}(m,x,t)\,dx\,dm\Bigg]+\Bigg[\int_{x_k-x_{k-3}}^{x_{k-5}}\int_{m_k-x}^{m_{k-3}}\mathcal{F}^J_{k-4,k-6}(m,x,t)\,dx\,dm$$
$$+\int_{x_{k-5}}^{x_{k-4}}\int_{m_k-x}^{m_{k-3}}\mathcal{F}^J_{k-4,k-5}(m,x,t)\,dx\,dm+0.5\int_{x_{k-4}}^{x_{k-3}}\int_{m_{k-4}}^{m_{k-3}}\mathcal{F}^J_{k-4,k-4}(m,x,t)\,dx\,dm\Bigg]. \tag{A8}$$

APPENDIX B: CONVERGENCE OF THE NUMERICAL SOLUTION TO THE EXACT SOLUTION

There is no rigorous mathematical proof of the uniqueness of a numerical solution of a general nonlinear integro–differential equation and of its convergence to the exact solution. In spite of that, it is shown, using mathematical logic, that in the present case the numerical solution converges to the exact solution when the spectral resolution is increased.

Melzac [16] proved that the KCE has a unique and exact solution when the initial distribution function is positive, continuous, bounded, and integrable and the kernel is symmetric and bounded. All these conditions are fulfilled in the present case. In addition, Drake [3]

showed that all the moments of the distribution function can be found using Mellen's transformation [25]. Once the moments are known, they can be used to calculate the actual distribution function. The accuracy of the calculated distribution function depends on the number of moments used in the calculation.

The inequality (7) for the nondimensional parameter ξ introduced by Tzivion *et al.* [26] is valid for all positive continuous functions and demonstrates that the range of values of ξ depends only on the parameter p. Therefore, the accuracy of the approximation for high moments by (9) depends on the value of p only.

For example, when $p=2$ the maximum error in the approximation of the second and fifth moments by the first two moments using (8) and (9) is 6.25 and 83%, respectively. For $p=2^{1/4}$ the errors sharply decrease to 0.38 and 3.83%, respectively. Therefore, any required degree of accuracy can be achieved by decreasing the value of p.

This implies that if one obtains the first two spectral moments with high accuracy then it is possible to get any other higher moment with any required accuracy by using an appropriate spectral resolution. In accordance with the work of Drake [3] which was discussed above, the distribution function itself can be determined.

Using the multi-moments method, a set of equations with respect to spectral moments of the distribution function is obtained from the original KCE without any mathematical or physical assumptions. This is done for $p=2$, $2^{1/2}$, $2^{1/3}$, and $2^{1/4}$ (Eqs. (A5)–(A8), respectively).

In order to solve this set of equations one approximates the distribution function in each spectral bin using its two first moments. In the present scheme, a power polynomial approximation is used that accurately calculates the moments used for the approximation and assures the positiveness of the distribution function. The order of the polynomial depends on the number of moments one wants to consider, the larger the number of moments, the higher the order of the polynomial approximation. In the present case linear or cubic approximations are used. Obviously, when one increases the spectral resolution, the approximation of the distribution function in the bin interval is closer to the actual distribution function. That means that in order to obtain a better approximation of the distribution function one can increase the spectral resolution or increase the order of the polynomial of the approximation.

As a result of the approximation, one obtains a set of equations in which the time-dependent functions are out of the integrals. The expressions under the integrals are of the type $m^j x^k \sigma(m, x)$, a known and time independent function, and can be calculated in advance up to machine precision accuracy.

Finally, a closed set of ordinary differential equations with respect to the first two spectral moments (Eq. (12)) is obtained. The accuracy of the numerical solution of these equations depends only on the spectral resolution and time step. For small time steps and high resolution the numerical solution approaches the exact solution [12, 14, 19]. While a significant difference is observed between the results for time steps of 10 s and 5 s, they are very similar for 5 s and 2 s and those for 2 s and 1 s are almost identical (Fig. 7).

When the spectral resolution is increased, the results gradually converge. Increasing the number of bins from 108 to 144 produces only a small difference in the results. This convergence is obtained for any initial conditions and kernels. Therefore, for 144 bins and time step of 1 s very accurate solutions for the first two spectral moments are obtained and one can proceed to find other higher moments with acceptable accuracy, using Eq. (9). Once these moments are known the distribution function itself can be constructed.

ACKNOWLEDGMENTS

Special thanks are due to Mrs. Zipi Rosen and Mrs. Sara Rehavi for their help with the programming and the testing of the code, without whom this work would have never been accomplished. Part of this work was conducted under a grant from the Water Commissioner of Israel as part of of the Rain Enhancement Project of Israel.

REFERENCES

1. E. X. Berry and R. L. Reinhardt, An analysis of cloud drop growth in collection: Parts 1 and 2, *J. Atmos. Sci*. **31**, 1814 (1974).
2. R. Bleck, A fast approximative method for integrating the stochastic coalescence equation, *J. Geohpys. Res*. **75**, 5165 (1970).
3. R. L. Drake, The scalar equation of coalescence theory: Moments and kernels, *J. Atmos. Sci*. **29**, 537 (1972).
4. I. M. Enukashvily, A numerical method for integrating the kinetic equation of coalescence and breakup of cloud droplets, *J. Atmos. Sci*. **37**, 2521 (1980).
5. D. Eyre and J. C. Wright, Spline-collocation with adaptive mesh grading for solving the stochastic collection equation, *J. Comput. Phys*. **38**, 288 (1988).
6. G. Feingold, S. Tzivion, and Z. Levin, The evolution of raindrop spectra. Part I. Stochastic collection and breakup, *J. Atmos. Sci*. **45**, 3387 (1988).
7. F. Gelbard and J. H. Seinfeld, Numerical solution of the dynamic equation for particulate systems, *J. Comput. Phys*. **28**, 357 (1978).
8. D. T. Gillespie, The stochastic coalescence model for cloud droplet growth, *J. Atmos. Sci*. **29**, 1496 (1972).
9. D. T. Gillespie, Three models for the coalescence growth of cloud drops, *J. Atmos. Sci*. **32**, 600 (1975).
10. D. T. Gillespie, An exact method for numerically simulating the stochastic coalescence process in a cloud, *J. Atmos. Sci*. **32**, 1977 (1975).
11. A. M. Golovin, The solution of the coagulation equation for cloud droplets in a rising air current, *Izv. Zkad. Nauk. SSSR Ser. Geofiz*. **5**, 783 (1963).
12. D. Greenspan and V. Casulli, Numerical analysis for applied mathematics, science, and engineering (Addison-Wesley, Reading, MA, 1988).
13. W. D. Hall, A detailed microphysical model within a two-dimensional dynamic framework: Model description and preliminary results, *J. Atmos. Sci*. **37**, 2486 (1980).
14. R. W. Hamming, *Numerical Methods for Scientists and Engineers* (McGraw–Hill, New York/San Francisco/Toronto/London, 1962).
15. A. B. Long, Solutions to the droplet coalescence equation for polynomial kernels, *J. Atmos. Sci*. **11**, 1040 (1974).
16. Z. A. Melzak, A scalar transport equation, *Trans. Amer. Math. Soc*. **85**, 547 (1957).
17. J. deJ. Montoya, A. J. C. Sampaio, and F. C. de Almeida, An analysis of the effect of decreasing the size resolution in two techniques to solve the stochastic collection equation for growing cloud drops, *Atmos. Res*. **35**, 173 (1995).
18. T. Reisin, Z. Levin, and S. Tzivion, Rain production in convective clouds as simulated in an axisymmetric model with detailed microphysics. Part I. Description of the Model, *J. Atmos. Sci*. **53**, 497 (1996).
19. R. D. Richtmayer and K. W. Morton, *Difference Methods for Initial-Value Problems* (Interscience, New York/London/Sydney, 1967).
20. B. C. Scott and P. V. Hobbs, On the connection between the Telford and kinetic-equation approaches to droplet coalescence theory, *J. Atmos. Sci*. **25**, 871 (1968).
21. B. C. Scott, Poisson statistics in distributions of coalescing droplets, *J. Atmos. Sci*. **24**, 221 (1967).
22. M. Seesselberg, T. Trautmann, and M. Thorn, Stochastic simulations as a benchmark for mathematical methods solving the coalescence equation, *Atmos. Res*. **40**, 33 (1996).
23. C. Seigneur, A. B. Hudischewskyj, J. H. Seinfeld, K. T. Whitby, E. R. Whitby, J. R. Brock, and H. M. Barnes, Simulation of aerosol dynamics: A comparative review of mathematical models, *Aerosol Sci. Technol*. **5**, 205 (1986).

24. M. Smoluchowski, *Brownian Motions*, Observatoria Nauchno Technicheskoi Informatzii (1936). [Russian]
25. I. N. Sneddon, *Fourier Transforms* (McGraw–Hill, New York, 1951).
26. S. Tzivion, G. Feingold, and Z. Levin, An efficient numerical solution to the stochastic collection equation, *J. Atmos. Sci*. **44**, 3139 (1987).
27. S. Tzivion, G. Feingold, and Z. Levin, The evolution of raindrop spectra. Part II. Collisional collection/breakup and evaporation in a rainshaft, *J. Atmos. Sci*. **46**, 3312 (1989).
28. B. M. Voloshtsuk and U. S. Sedunov, *Coagulation Processes in Disperse Systems* (Gydrometeoizdat, Leningrad, 1975). [Russian]